Analysis of Reaction Rates in the Cathode Electrode of Polymer Electrolyte Fuel Cell I. Single-Layer Electrodes

Yun Wang*,z and Xuhui Feng

Renewable Energy Resources Lab and National Fuel Cell Research Center, Department of Mechanical and Aerospace Engineering, The University of California, Irvine, Irvine, California 92697-3975, USA

This paper explores transport and electrochemical phenomena in the cathode electrode of polymer electrolyte fuel cells and presents a theoretical study on the spatial distribution of reaction rates across the electrode. Profiles of the electrolyte-phase potential and local electrochemical reaction rate are explicitly obtained and related to a variable ΔU_δ, which lumps the impacts of a number of parameters including composite properties, electrode structure, and other factors such as oxygen concentration and water content. Spatial variations of the local reaction current are analyzed and impacts of the parameters are investigated. Finally, a variable, the reaction rate nonuniformity $\hbar$, is defined based on average current density and is found to vary linearly with another lumped parameter ΔU, which combines the effects of average current density and ionic conductivity. It is also found $\hbar$ can be used to approximate the current density contribution of each portion of the electrode if the electrode is divided by half.
© 2008 The Electrochemical Society. [DOI: 10.1149/1.2988763] All rights reserved.

The cathode electrode or catalyst layer of polymer electrolyte fuel cells (PEFCs) is of paramount importance for PEFC performance. In the cathode, the oxygen reduction reaction (ORR) takes place at the triple-phase boundaries (TPBs), which is laggard and therefore leads to a considerable voltage loss. Currently, precious metals such as platinum and its alloy are the best candidates as the catalyst for the ORR. Therefore, fundamental understanding of the reaction kinetics in the electrode, e.g., spatial distribution of local reaction current, is crucial for development of cost-effective high-performance fuel cells.

Both experimental and numerical studies have been conducted to investigate the transport and electrochemical phenomena in the electrode as well as the electrode's performance and optimization. Springer et al.[1,2] formulated a one-dimensional (1D) model to elucidate water transport and electrochemical processes in fuel cells. They experimentally determined the formula to relate membrane water content to membrane properties such as ionic conductivity and water diffusion coefficient. Boyer et al.[3] investigated the effective ionic conductivity in the electrode and found it is proportional to the Nafion content. Impacts of Nafion loading on the electrode ionic conductivity were investigated by Li and Pickup[4] via impedance spectroscopy, cyclic voltammetry, and polarization experiments. They observed that the highest electronic resistances appear at low Nafion loadings and suggest Nafion plays an important role as a binder. Neyerlin et al.[5] conducted both theoretical analysis and an experimental study to investigate catalyst utilization in the cathode. A factor characterizing the catalyst utilization is defined for electrode design and fabrication.

Numerical and modeling work has been conducted by several studies. Boyer et al.[6] presented a formula for electrode optimization. They investigated impacts of several parameters such as catalyst thickness, Nafion content, and catalyst loading. A model for the fuel cell cathode side was developed by Gurau et al.[7] which includes transport mechanisms in the electrode. Wang and Wang[8] developed a computational fluid dynamics based fuel cell model and studied the transport phenomena within the electrodes. Reaction-induced velocity distributions were obtained in both catalyst layers and diffusion media. Several nonisothermal[9,10] and two-phase[11-15] models were developed to study various heat generation mechanisms and two-phase transport in fuel cell components including electrodes. Wang and Wang[16] developed a transient model for polymer electrode membrane (PEM) fuel cells that describes the hydration process in the membrane phase of electrodes. Eikerling[17] presented a structure-based model to study the water management in the electrode. They use effective properties based on the statistical theory of

random composite media in their model. Wang and Wang[18] predicted a remarkable undershoot in cell voltage during transient through examining the evolutions of water activity and ionic resistance in the electrode. Wang et al.[19] applied the Poisson–Nernst–Planck theory for proton transport in the electrode and investigated electrode potential and reaction rates as well as catalyst utilization. Das et al.[20] developed a fuel cell model to relate electrode parameters such as platinum loading and electrode thickness to cell performance. Weber and Newman[21] numerically investigated the impact of the cathode thickness on cell performance and concluded that the electrode thickness distributions have little effect on overall cell performance. Wang et al.[22] presented a detailed study on cathode performance via direct numerical simulation and predicted the optimal porosity and electrolyte volume fraction for the electrode. Wang[23] conducted a study on transport and electrochemical phenomena during cold-start and identified the key parameters affecting the electrode performance in cold-start.

Despite the efforts in previous studies, analytical solutions of electrochemical reaction rates within electrodes are highly desirable, particularly those that explicitly relate the electrode local performance to the key parameters such as electrode composition and structural features. In this paper, we analyze heat and species transport in the electrode and develop a 1D model to investigate the electrochemical kinetics in the cathode. Analytical solutions are explicitly obtained for the profiles of electrolyte-phase potential and reaction current in the cathode electrode. Factors that affect the profiles are investigated.

Modeling and Theoretical Analysis

Electrochemical kinetics in the cathode electrode.— Figure 1 schematically shows the fuel cell structure and electrode. Electrodes are the thin layers (~ 10 μm) coated on the membrane surface, containing catalyst (typically platinum), carbon, ionomer electrolyte, and void space. Nanoparticles of catalyst platinum attach on the surface of supporting carbon powders with electrolyte ionomer covering on the surfaces, forming the TPBs. Carbon powders are the media for electron transport while protons travel through the electrolyte phase. Electrochemical reactions, hydrogen dissociation, and
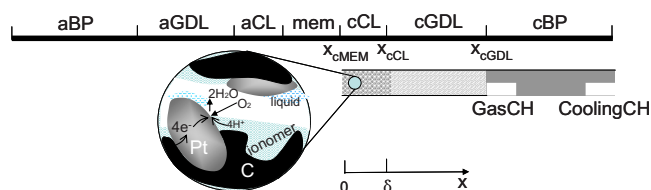
* Electrochemical Society Active Member.
z E-mail: yunw@uci.edu

Figure 1. (Color online) Schematic of the cathode electrode.

ORRs take place at the TPBs, with water and heat as the only by-products. Transport of species such as hydrogen and oxygen occurs primarily in the void space while water transports in both electrolyte and void phases. In the cathode, the ORR takes place at the TPBs

$$O_2 + 4e^- + 4H^+ \rightarrow 2H_2O + Heat \quad [1]$$
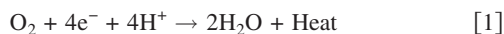
The electrochemical reaction rate can be obtained by the Butler–Volmer equation. As the ORR sluggish kinetics results in high cathode overpotential, the Butler–Volmer equation can be well approximated by Tafel kinetics

$$j = - ai_{0,T}^{\text{ref,c}} \left(\frac{C_{O_2}}{C_{O_2}^{\text{ref}}} \right) \exp\left(- \frac{\alpha_c F}{R_g T} \eta \right) \quad [2]$$

where the surface overpotential is defined as

$$\eta = \Phi^{(s)} - \Phi^{(m)} - U_o \quad [3]$$

where $\Phi^{(s)}$ and U_o are the electronic phase potential and equilibrium potential, respectively. Typically, the electrode electronic conductivity is high, thus, variation of $\Phi^{(s)}$ can be neglected. U_o is a function of temperature

$$U_o = 1.23 - 0.9 \times 10^{-3}(T - 298) \quad [4]$$

The electrolyte phase potential, $\Phi^{(m)}$, can be modeled by neglecting electrochemical double-layer charging/discharging

$$\nabla \cdot (\sigma_m^{\text{eff}} \nabla \Phi^{(m)}) + j = 0 \quad [5]$$

The ionic conductivity, σ_m^{eff}, is determined by the electrolyte water content, λ, in the electrode and composite properties such as Nafion content ε_m and tortuosity of the ionomer τ_m (Ref. 1)

$$\sigma_m^{\text{eff}} = \varepsilon_m^{\tau_m}(0.5139\lambda - 0.326)\exp\left[1268\left(\frac{1}{303} - \frac{1}{T}\right)\right] \quad [6]$$

In addition, temperature and liquid water affect the ORR and the exchange current density, $ai_{0,T}^{\text{ref,c}}$, can be expressed in Arrhenius form[23,24]

$$ai_{0,T}^{\text{ref,c}} = ai_0^{\text{ref,c}}(1 - s)\exp\left[- \frac{E_a}{R_g}\left(\frac{1}{T} - \frac{1}{353.15}\right)\right] \quad [7]$$

where E_a denotes the activation energy for ORR at the Pt/Nafion electrode and s is the liquid water saturation. Note that the value of the exchange current density is also related to several factors such as Pt loading and electrode roughness. Table I lists the typical values of several parameters related to the above equations.

Heat transfer in the cathode electrode.— A major part of the heat generation in fuel cells comes from the reaction heat $j[\eta + T(dU_o/dT)]$, which occurs at the reaction surface in the electrode. Heat may also be added due to the Joule heating arising from the ohmic resistance and latent heat during phase change. Estimating the magnitude of temperature variation across the electrode can be performed by assuming all the heat is generated in the electrode[23]

$$\Delta T \sim \frac{\delta^2 S_T}{k^{\text{eff}}} = \frac{\delta(E_o - V_{\text{cell}})I}{k^{\text{eff}}} \quad [8]$$

where the total heat generation rate has been approximated by $(E_o - V_{\text{cell}})I$ with E_o being the thermodynamic equilibrium cell potential. The effective conductivity k^{eff} of 3.0 W/m K yields $\Delta T \approx 0.03$ K at 1.0 A/cm^2, which is small and therefore leads to a negligible variation of U_o and $ai_{0,T}^{\text{ref,c}}$ across the electrode (see Eq. 4 and 7).

Oxygen transport in the cathode electrode.— Oxygen transport in the electrode is driven by both convection and diffusion. Convection is induced by mass consumption/production of the electrochemical reaction and can be neglected comparing with diffusion.[8] Two diffusive mechanisms need to be considered in the electrode; the Knudson diffusion and the molecular one. The Knudson diffusion becomes important when the mean-free path of gas molecules

is of the order of the pore characteristic length scale. In the electrode, the mean pore radius in the electrode is typically ~0.1 μm and the related Knudsen diffusion coefficient can be obtained through the kinetic theory of gases, which is around 3.0 × 10^{-5} m^2/s.[23] In addition, the molecular diffusion also takes place and its coefficient is a function of temperature and pressure

$$D_{M,O_2} = D_{M,O_2,0} \left(\frac{T}{353} \right)^{3/2} \left(\frac{1}{P} \right) \quad [9]$$

Note that the Knudsen diffusion coefficient is comparable to the molecular one. We apply the harmonic mean to combine these two mechanisms and further modify the diffusion coefficient by considering the parameters of porosity ε and tortuosity τ as well as liquid water saturation s[23]

$$D_{O_2}^{\text{eff}} = \frac{\varepsilon(1 - s)}{\tau} D_{O_2} = [\varepsilon(1 - s)]^{\tau_d} D_{O_2} \quad [10]$$

By neglecting the convection effect, the magnitude of oxygen concentration variation across the electrode can be estimated by[23]

$$\Delta C_{O_2} \approx \frac{I}{8F} \frac{\delta}{D_{O_2}^{\text{eff}}} \quad [11]$$

Typical values of the parameters, i.e., $D_{O_2}^{\text{eff}}$ of 10^{-5} m^2/s and δ of 10^{-5} m, will yield ΔC^{O_2} of ~0.02 mol/m^3 even at 1.0 A/cm^2, which is quite small and can be safely neglected in most ranges of fuel cell operation.

Characterization of water transport in the cathode electrode.— In the composite electrode, water is transported in both electrolyte phase and void space. In the void space, water may exist in gaseous and liquid phases and is primarily delivered by diffusion and capillary action, respectively.

No liquid water region.— When no liquid is present, water is transported by diffusion in both electrolyte and gaseous phases. The water diffusion coefficient in the electrolyte was experimentally determined by Motupally et al.[25]

$$D_{H_2O}^{(m)} = \begin{cases} 3.1 \times 10^{-3}\lambda(e^{0.28\lambda} - 1)e^{[-2436/T]} & \text{for } 0 < \lambda \leq 3 \\ 4.17 \times 10^{-4}\lambda(1 + 161e^{-\lambda})e^{[-2436/T]} & \text{otherwise} \end{cases}$$
$$[12]$$

The gaseous diffusion coefficient can be expressed in a form similar to the one of oxygen. By assuming the thermodynamic equilibrium between electrolyte and gas phases, water transport in these two phases can be combined by defining an effective diffusion coefficient

$$D_{H_2O}^{\text{eff}} = D_{H_2O}^{(g),\text{eff}} + D_{H_2O}^{(m),\text{eff}} = \varepsilon^{\tau_d}D_{H_2O}^{(g)} + \varepsilon_m^{\tau_m}D_{H_2O}^{(m)}\frac{dC_{H_2O}^{(m)}}{dC_{H_2O}} \quad [13]$$

where $C_{H_2O}^{(m)}$ is the molar concentration of water in the membrane phase, and $D_{H_2O}^{(m),\text{eff}}$ is the modified diffusion coefficient for water diffusion through the ionomer if expressed in terms of the gradient in the gas-phase molar concentration. The Bruggeman correlation is applied here to account for the tortuosity effect. Again, neglecting the convection effect, the water concentration variation across the electrode can be estimated by a formula similar to the oxygen, as shown in Eq. 11

$$\Delta C_{H_2O} = \frac{(1 + 2n_d)I}{4F} \frac{\delta}{D_{H_2O}^{\text{eff}}} \quad [14]$$

Typical values of the parameters, e.g., the electro-osmotic drag coefficient $n_d \approx 1.0$, yield a small concentration variation of ~0.08 mol/m^3 at 1.0 A/cm^2, which can only lead to a fairly small change of the ionic conductivity σ_m^{eff} across the electrode. Details of the relationship between the ionic conductivity and water activity in the membrane can be found in Ref. 1.

Liquid water region.— Liquid water emerges when the water gaseous partial pressure reaches the saturation value. Again, by assuming thermodynamic equilibrium between the gaseous and liquid phases, one can conclude that the gaseous diffusion is negligible as the temperature variation is small (see Eq. 8), therefore leading to a nearly uniform water partial pressure across the electrode. Liquid water transport in the void is primarily driven by capillary pressure, which can be treated similar to diffusive mechanisms with the "diffusion" coefficient[12,26]

$$D_c^{(l)} = -\frac{k_{rl}}{\nu^{(l)}}\sigma\,\cos(\theta_c)(K\varepsilon)^{1/2}\frac{dJ(s)}{ds} \qquad [15]$$

where k_{rl} is the relative permeability for liquid and physically describes the extent to which the liquid flow is hindered by the gaseous one in pore spaces and hence, can be formulated as a function of liquid saturation. Most previous work, including this paper, adopts a cubic relation. $J(s)$ is the empirical Leveret-J function and is given by

$$J(s) = 1.417s - 2.120s^2 + 1.263s^3 \qquad [16]$$

Note that $D_c^{(l)}$ is a function of the liquid saturation and porous media properties. The liquid water saturation variation Δs across the cathode electrode can then be estimated by

$$\Delta s = \frac{(1 + 2n_d)I}{4F}\frac{\delta}{D_c^{(l)}}M_{H_2O} \qquad [17]$$

In the range of $5\% < s < 80\%$, typical values of the parameters, e.g., K of 10^{-14} m^2, θ_c of 120°, and k_{rl} of s^3, yield a variation of liquid saturation $\sim 1\%$ at 1 A/cm^2, which is quite small and therefore can be neglected in most ranges of fuel cell operation. Note that the upper limit of the range, 80%, is well above the one that can occur in an operating fuel cell (which is typically <30 to 40%). In addition, from Eq. 7, one can assume a uniform exchange current density, $ai_{0,T}^{ref,c}$, across the cathode electrode due to the small spatial variations of s and temperature T if other factors, such as Pt loading, are uniform.

Further, liquid saturation may also affect oxygen transport in the electrode. Even with 40% of the liquid saturation, the oxygen concentration variation is still small across the electrode, which can be estimated by Eq. 14. Small oxygen concentration variation in the electrode is not directly related to the mass-transport limitation of fuel cells which is primarily governed by the oxygen transport within the gas diffusion layer (GDL) or spatial variation of oxygen concentration across the GDL. Again, the conclusion drawn from this analysis is to show that the oxygen concentration across the catalyst layer can be assumed constant, even considering the presence of liquid water in a typical PEFC. Therefore, this assumption can be adopted to simplify the model of the electrochemical reaction for exact solutions in wide range of fuel cell operation. As to higher saturation such as 50–90%, it rarely happens in a typical fuel cell and should be avoided in practice if possible. Therefore, we exclude our discussion in that range.

Analytical solutions.— The above analysis indicates that the oxygen and water concentrations, liquid water saturation, ionic conductivity, temperature, and electronic phase potential can be assumed uniform across the cathode electrode (or in the x direction) in most of the ranges of fuel cell operation. Considering the cathode electrode in one dimension (x direction) as shown in Fig. 1, substituting Eq. 2 into Eq. 5 yields

$$\frac{d^2}{dx^2}\Phi^{(m)} = \frac{ai_{0,T}^{c,ref}}{\sigma_m^{eff}}\frac{C_{O_2}}{C_{O_2}^{ref}}\exp\left(-\frac{\alpha_c F}{R_g T}(\Phi^{(s)} - U_o - \Phi^{(m)})\right) \qquad [18]$$

By considering the following boundary conditions

Table I. Physical parameters.

Quantity	Value
Porosity/tortuosity of electrodes, ε/τ_d	0.5/1.5
Exchange current density × reaction surface area, $ai_0^{ref,c}$	10,000 A/m^3
Volume fraction/tortuosity of ionomer in electrodes, ε_m/τ_m	0.20/1.5
Transfer coefficient, α_c	1
O$_2$/H$_2$O molecular diffusivity in the cathode at standard condition, $D_{M,O_2,0}/D_{M,H_2O,0}$	$3.2348 \times 10^{-5}/3.89 \times 10^{-5}$ m^2/s
Viscosity of liquid water, $\mu^{(l)}$	3.5×10^{-4} kg/m s
Density of dry membrane, ρ_m	1980 kg/m^3
Surface tension, liquid–water–air (80°C), σ	0.0625 N/m
Ew (equivalent weight)	1.1
Activation energy for oxygen reduction reaction, E_a	73,269 J/mol

$$\Phi^{(m)} = \Phi_\delta^{(m)} \quad \text{and} \quad \frac{d}{dx}\Phi^{(m)} = 0 \quad \text{at } x = \delta \qquad [19]$$

the solution to the above 1D problem can be explicitly given by

$$\Phi^{(m)} = \frac{R_g T}{\alpha_c F}\ln\left\{\left[\tan\left(\pm\left[-\frac{\alpha_c F}{2R_g T}\frac{j_\delta \delta^2}{\sigma_m^{eff}}\right]^{1/2}\frac{\delta - x}{\delta}\right)\right]^2 + 1\right\} + \Phi_\delta^{(m)} \qquad [20]$$

where

$$j_\delta = j(x = \delta) \qquad [21]$$

$j(x)$ is calculated by Eq. 2. Physically, j_δ represents the transfer current density at the interface of diffusion media and electrode, i.e., $x = \delta$. To simplify Eq. 20, we define the following parameters

$$I^{j\delta} = -j_\delta \delta \quad R_\delta = \frac{\delta}{\sigma_m^{eff}} \quad \Delta U^{j\delta} = R_\delta I^{j\delta} \qquad [22]$$

Physically, $I^{j\delta}$ represents the current density based on the transfer current density j_δ at the interface between the electrode and diffusion media, while R_δ is the overall ionic resistance across the cathode electrode. (Note that σ_m^{eff} is almost constant across the electrode.) The lumped variable $\Delta U^{j\delta}$ contains the impacts of a number of parameters, such as electrode composition and structural properties, e.g., the Nafion content ε_m, platinum loading, tortuosity τ, and porosity (see Eq. 6 and 7), and other physical parameters, e.g., oxygen concentration and water content (see Eq. 21). Some of the parameters such as platinum loading and Nafion content are the key factors for electrode fabrication and performance/cost optimization. Then the expression of $\Phi^{(m)}$ can be rewritten as a function of $\Delta U^{j\delta}$

$$\Phi^{(m)} = \frac{R_g T}{\alpha_c F}\ln\left\{\left[\tan\left(\pm\left[\frac{\alpha_c F}{2R_g T}\Delta U^{j\delta}\right]^{1/2}\frac{\delta - x}{\delta}\right)\right]^2 + 1\right\} + \Phi_\delta^{(m)}$$

$$= \frac{R_g T}{\alpha_c F}\ln\{\Pi(\Delta U^{j\delta}, \bar{x}) + 1\} + \Phi_\delta^{(m)} \qquad [23]$$

where

$$\Pi(\Delta U^{j\delta}, \bar{x}) = \left[\tan\left(\pm\left[\frac{\alpha_c F}{2R_g T}\Delta U^{j\delta}\right]^{1/2}(1 - \bar{x})\right)\right]^2 \quad \text{and} \quad \bar{x} = \frac{x}{\delta} \qquad [24]$$

Equation 23 can also be rearranged to describe the overpotential variation $\Delta\eta$ within the cathode by considering the fact that electronic phase potential $\Phi^{(s)}$ and U_0 are almost uniform across the electrode

$$\Delta\eta(\bar{x}) = \Phi^{(m)}(\bar{x}) - \Phi_\delta^{(m)} = \frac{R_g T}{\alpha_c F} \ln\{\Pi(\Delta U^{j\delta}, \bar{x}) + 1\} \quad [25]$$

where $\Delta\eta$ represents the overpotential difference between the location $\bar{x}$ and the interface between the electrode and diffusion media, i.e., $\bar{x} = 1$.

By using Eq. 2 and 23, the local transfer current can be calculated by

$$j(\bar{x}) = j_\delta[\Pi(\Delta U^{j\delta}, \bar{x}) + 1] \quad \text{or} \quad \frac{j(\bar{x}) - j_\delta}{j_\delta} = \Pi(\Delta U^{j\delta}, \bar{x}) \quad [26]$$

A typical location is the other interface, i.e., the one between the membrane and cathode, and the transfer current density j_0 can be obtained by setting $\bar{x} = 0$ for the above equation

$$\frac{j_0 - j_\delta}{j_\delta} = \Pi(\Delta U^{j\delta}, 0) \quad [27]$$

As the function of $\Pi(\Delta U^{j\delta}, \bar{x})$ monotonously increases with $1 - \bar{x}$ in the range considered, the value of $\Pi(\Delta U^{j\delta}, 0)$ can be used to assess the uniformity of local electrochemical reaction in the depth-direction of the electrode, which only depends on one lumped variable $\Delta U^{j\delta}$, as shown in Eq. 27. The drawback of using $\Delta U^{j\delta}$ is that it is not a quantity directly obtained from experiment.

Given the $\Phi^{(m)}$ distribution, the average current density I, a key parameter characterizing fuel cell performance, can be obtained by

$$I = -\sigma_m^{eff} \left.\frac{d\Phi^{(m)}}{dx}\right|_{\bar{x}=0} \quad [28]$$

Substituting Eq. 23 yields

$$I = \left(2\frac{\sigma_m^{eff} R_g T}{\alpha_c F}\right)^{1/2} (j_\delta - j_0)^{1/2} \quad [29]$$

The above can be further rewritten as

$$I = \left(2\frac{\sigma_m^{eff} R_g T}{\alpha_c F} j_\delta\right)^{1/2} \tan\left[\left(\frac{\alpha_c F}{2R_g T}\frac{j_\delta \delta^2}{\sigma_m^{eff}}\right)^{1/2}\right] \quad [30]$$

The above equation relates the average current density I to the transfer current at the interface between the electrode and diffusion media j_δ. In most cases, the average current density I is an input parameter. The above equation can then be employed to obtain the transfer current at the interface j_δ implicitly. The obtained j_δ can further be used to calculate the analytical solutions of transfer current density and electrolyte phase potential distributions by Eq. 26 and 23, respectively.

By using the parameters defined in Eq. 22, one can further rewrite the average current as

$$I = \left[2\frac{R_g T}{\alpha_c F}\frac{\Delta U^{j\delta}}{R_\delta^2}\right]^{1/2} \left|\tan\left(\pm\left[\frac{\alpha_c F}{2R_g T}\Delta U^{j\delta}\right]^{1/2}\right)\right|$$

$$= \left[2\frac{R_g T}{\alpha_c F}\frac{\Delta U^{j\delta}}{R_\delta^2}|\Pi(\Delta U^{j\delta}, 0)|\right]^{1/2} \quad [31]$$

Instead of using $\Pi(\Delta U^{j\delta}, 0)$ as a factor indicating the degree of local reaction spatial variation, we choose the average current I as the scale and define a variable $\hbar$ to quantify the nonuniformity of the reaction rate

$$\hbar = \frac{|j_0 - j_\delta|}{\int_0^1 j(\bar{x})d\bar{x}} = \frac{|j_0 - j_\delta|}{\frac{I}{\delta}} \quad [32]$$

It can be seen that the smaller the value of $\hbar$, the more uniform the transfer current across the electrode. The significance of the parameter $\hbar$ is that it quantifies the degree of reaction variation across the electrode, which is an important factor assessing electrode performance and therefore can be applied to both theoretical and numerical studies of the electrode process. For example, the assumption of
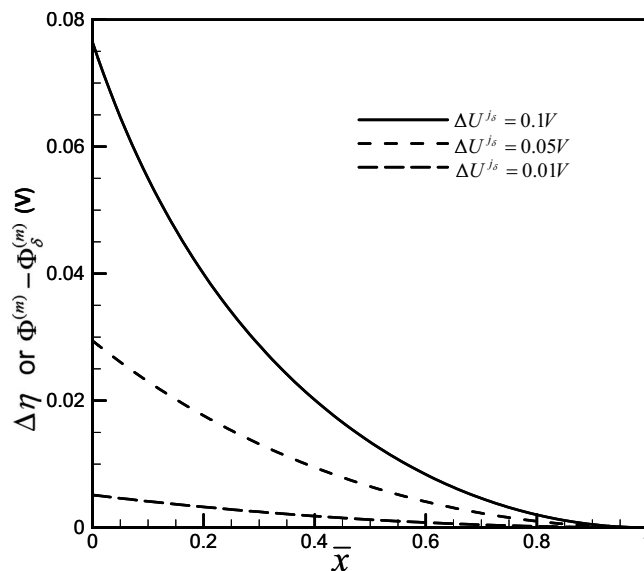

Figure 2. Profiles of $\Delta\eta$ or $\Phi^{(m)} - \Phi_\delta^{(m)}$ in the cathode electrode at different $\Delta U^{j\delta}$ values.

uniform reaction rate is frequently adopted in electrode analysis. $\hbar$ can be used to assess the validity of this assumption. In addition, in the area of multidimensional modeling and numerical simulation, $\hbar$ can be used for developing efficient electrode models and numerical tools, e.g., in cases of small $\hbar$ where the reaction can be treated uniform across the electrode, the model can be improved to use only one reaction rate variable to describe the electrode performance in the thickness dimension.

By substituting Eq. 29 into 32, one will obtain

$$\hbar = \frac{I\delta}{2\frac{\sigma_m^{eff} R_g T}{\alpha_c F}} \quad [33]$$

which indicates that $\hbar$ is a function of the average current density, electrode thickness, ionic conductivity, and temperature. In particular, when the electrode temperature and thickness are fixed, the degree of uniformity of the reaction rate is determined by the ionic conductivity and average current density only. A lumped parameter ΔU can further be defined similar to Eq. 22 as

$$\Delta U = \frac{I\delta}{\sigma_m^{eff}} = IR_\delta \quad [34]$$

Physically, ΔU indicates the magnitude of the electrolyte phase potential drop across the electrode. Note that it only depends on two parameters key to electrode performance, i.e., the electrode ionic resistance and average current density. The definition of ΔU can further simplify Eq. 33 by

$$\hbar = \frac{\Delta U}{2\frac{R_g T}{\alpha_c F}} \quad [35]$$

Results and Discussion

Figure 2 shows profiles of the overpotential variation $\Delta\eta$ or electrolyte potential variation $\Phi^{(m)}(\bar{x}) - \Phi_\delta^{(m)}$ in the cathode electrode. It can be seen that the overpotential is nonuniform within the cathode and particularly at high values of the lumped parameter $\Delta U^{j\delta}$, the spatial variation is significant. As $\Delta U^{j\delta}$ consists of two parts, δ/σ_m^{eff} and $j_\delta\delta$, for a specific electrode, the overpotential difference or electrolyte phase potential variation is only determined by the ionic diffusivity and transfer current density j_δ at the interface $\bar{x} = 1$: the
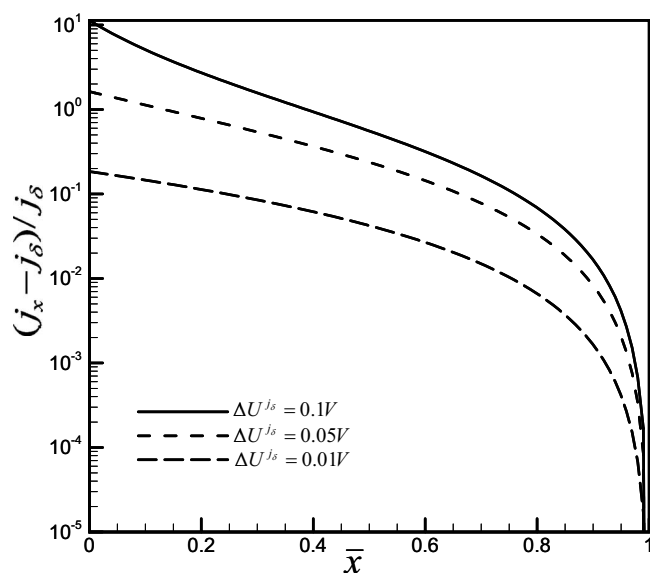
Figure 3. Profiles of local transfer current densities at different $\Delta U^{j\delta}$ values.

Figure 5. The average current density I vs $\Delta U^{j\delta}$ at different ionic resistances of the cathode electrode.

smaller the value of σ_m^{eff} or the higher the j_δ (which is determined by a number of factors such as oxygen concentration and local overpotential), the larger the overpotential or electrolyte phase potential variation will be.

Figure 3 shows the profiles of normalized local transfer current densities at different $\Delta U^{j\delta}$ values, i.e., Eq. 26. It can be seen that the electrochemical reaction rate is nonuniform in the electrode, with a higher value near the membrane side. In addition, at the value of $\Delta U^{j\delta}$ equal to 0.1 V (e.g., $I_\delta \approx 1.0$ A/cm^2, $\sigma_m^{eff} \approx 1.0$ S/m, or $I_\delta \approx 0.1$ A/cm^2, $\sigma_m^{eff} \approx 0.1$ S/m), the current density at the interface of the membrane side ($\bar{x} = 0$) is $\sim$10 times higher than the other side, i.e., $\bar{x} = 1$. When $\Delta U^{j\delta}$ is reduced to $\sim$0.01 V (e.g., $I_\delta \approx 0.1$ A/cm^2 and $\sigma_m^{eff} \approx 1.0$ S/m), the difference diminishes to within 20%. The trend also indicates that the lower the $\Delta U^{j\delta}$ value, the more uniform the reaction rate in the electrode.

Figure 4 shows the difference between the transfer current densities at several typical locations. It can be seen that the difference
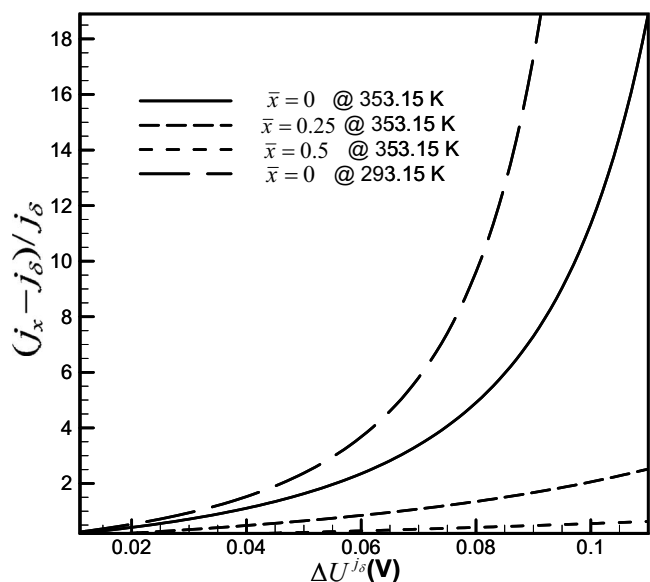

Figure 4. Transfer current densities at typical locations ($\bar{x} = 0$, 0.25, and 0.5) as a function $\Delta U^{j\delta}$.
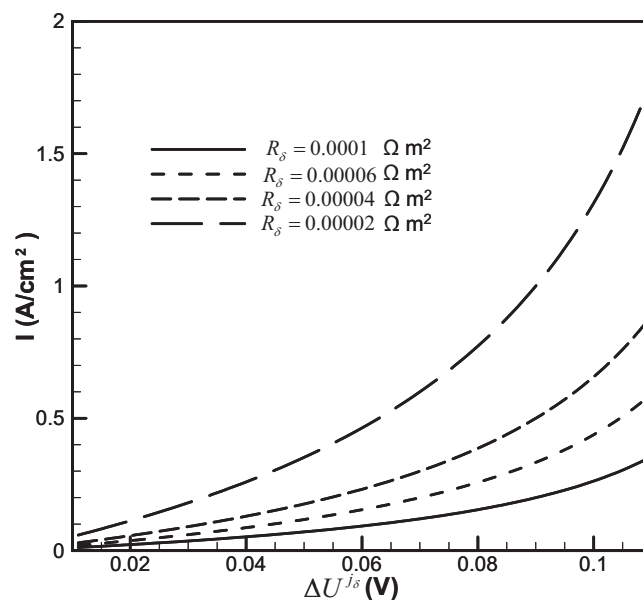
between the two interfaces, i.e., $\bar{x} = 0$, increases rapidly with $\Delta U^{j\delta}$ for the two temperatures considered. At the middle section, the reaction current shows a moderate increase (within 50%) from the one at $\bar{x} = 1$ in the range of $\Delta U^{j\delta}$ considered. At low values of $\Delta U^{j\delta}$ (either low I_δ or high σ_m^{eff}), the difference is quite small for all the cases. As $\Delta U^{j\delta}$ increases beyond 0.03 V, the reaction rate at the interface of the membrane side is raised more than two times than the one at the other interface. At high $\Delta U^{j\delta}$ values, even a small change, e.g., from 0.1 to 0.11 V, will significantly increase the difference of the reaction rates between the two interfaces. At the temperature of 293.15 K, the variation is much larger than the one at the higher temperature, particularly for large $\Delta U^{j\delta}$ values.

Figure 5 plots the relation between the average current density and the lumped parameter $\Delta U^{j\delta}$, i.e., Eq. 31. It can be seen that $\Delta U^{j\delta}$ is small at low current densities. In addition, for the electrode ionic resistance of 1.0 Ω cm^2 (e.g., $\sigma_m^{eff} \approx 0.1$ S/m and $\delta \approx 10^{-5}$ m), the current density I remains low even when the lumped parameter of $\Delta U^{j\delta}$ increases to over 0.1 V. For the 0.2 Ω cm^2 (e.g., $\sigma_m^{eff} \approx 0.5$ S/m) value, the current density of 1.3 A/cm^2 leads to 0.1 V of $\Delta U^{j\delta}$. In practice, the average current is usually an input parameter. From this plot or Eq. 31, $\Delta U^{j\delta}$ can be calculated from I, and the obtained value of $\Delta U^{j\delta}$ can be further used to calculate the distributions of local reactant rate and electrolyte phase potential.

Figure 6 plots the nonuniformity factor $\hbar$ of the reaction current, as defined by Eq. 33, in the cathode at two typical temperatures, 353.15 and 293.15 K, for the ordinary range of fuel cell operation. It can be seen that the reaction rate is more uniform at low ΔU values, (e.g., low average current density or high electrode ionic conductivity). At a fixed σ_m^{eff} in an electrode, the spatial variation of the electrode reaction rate is solely dependent on the average current I. Also, when I and temperature are set constant, the value of $\hbar$ is determined by the electrode ionic conductivity only. In addition, at lower temperatures the spatial variation of reaction currents is more sensitive to ΔU. Finally, this figure shows the factor $\hbar$ in the range from 0 to around 2, which is small compared with Fig. 4 due to different scales considered in the definitions of the two quantities, see Eq. 26. Figure 7 presents profiles of normalized transfer current density at different values of $\hbar$ within the cathode electrode. It can be seen that the degree of variation of $j(\bar{x})$ increases with the value of $\hbar$. From
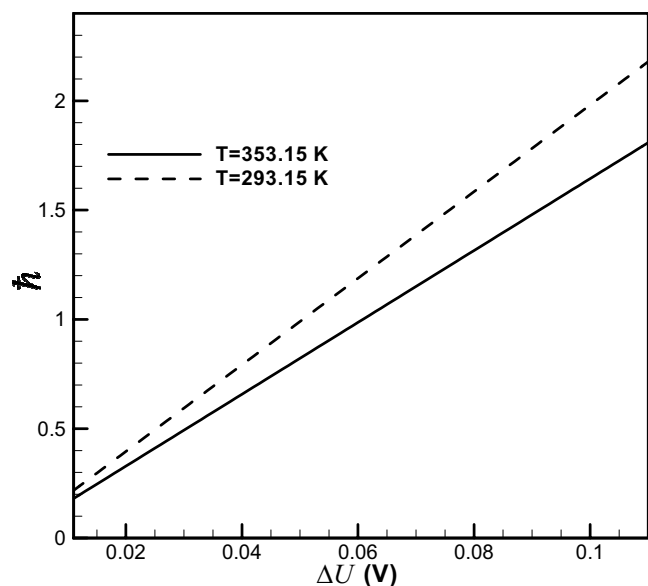
Figure 6. The nonuniformity factor, $\hbar$, in the cathode electrode.

$$\frac{\delta}{I}\int_0^{0.5}|j(\bar{x})|d\bar{x} \approx \frac{\delta}{4I}|j(0)+j(0.5)| \quad \text{and}$$

$$\frac{\delta}{I}\int_{0.5}^{1}|j(\bar{x})|d\bar{x} \approx \frac{\delta}{4I}|j(0.5)+j(1)| \qquad [36]$$

Note that $j(0)=j(\bar{x}=0)=j_0$ and $j(1)=j(\bar{x}=1)=j_\delta$. The right sides of the above equation can also be found in the $\hbar$ value definition (Eq. 32)

$$\hbar = \frac{\delta|j_0-j_\delta|}{I} = \frac{\delta}{I}|j(0)+j(0.5)| - \frac{\delta}{I}|j(0.5)+j(1)|$$

$$\approx \frac{4\delta}{I}\int_0^{0.5}|j(\bar{x})|d\bar{x} + \frac{4\delta}{I}\int_{0.5}^{1}|j(\bar{x})|d\bar{x} \qquad [37]$$

By considering the sum of the two terms in Eq. 36 is equal to 1, one will reach

$$\frac{\delta}{I}\int_0^{0.5}|j(\bar{x})|d\bar{x} \approx 0.5 + \frac{\hbar}{8} \quad \text{and} \quad \frac{\delta}{I}\int_{0.5}^{1.0}|j(\bar{x})|d\bar{x} \approx 0.5 - \frac{\hbar}{8}$$

$$[38]$$

Using the case of $\hbar = 1.97$ in Fig. 7 as an example, the current contribution from the portion of $\bar{x} = (0,0.5)$ is ~75%, while the other half is 25%. It can be seen that if the electrode is divided by half, the value of $\hbar$ is directly related to the performance of each half electrode. It is also worthy to note that the above conclusion is drawn by assuming a linear profile during integral, which is a better approximation at lower $\hbar$ values as shown in Fig. 7. As $\hbar$ approximates 4, Eq. 38 becomes invalid due to the increasing errors arising from this assumption.

Further, Fig. 7 clearly shows the physical meaning of $\hbar$, i.e., the degree of spatial variation of the reaction rate. In practice, $\hbar$ can be used to guide the electrode optimization. For example, at small $\hbar$ values which may take place in fuel cells with low currents or high humidity, e.g., glucose fuel cells and methanol fuel cells, the reaction rate is almost uniform across the electrode; therefore, a single-layer configuration may be sufficient. At large $\hbar$ values, which may be encountered for fuel cells with high currents or low humidity, e.g., PEM fuel cells for automobile application, the multiple-layer electrode may be applied to enhance the local catalyst utilization. We will continue addressing how to optimize the multiple-layer configuration in our second paper in this series.

the definition of $\hbar$, one can readily obtain $\hbar$ from this figure by calculating the difference of $j(\bar{x})$ between the two interfaces, i.e., $\bar{x} = 0$ and 1.

In addition, with the aid of Fig. 7, one can further explore the significance of the lumped parameter $\hbar$ in the electrode fundamental study. Physically, the integral of the variable at the y axis, i.e., $|j(\bar{x})|\delta/I$, from 0 to $\bar{x}$ (or the area between the curve and x axis) represents the portion of performance contributed by the part of electrode from 0 to x. The reaction current produced by the half portion of the electrode close to the electrolyte can be expressed by $(\delta/I)\int_0^{0.5}|j(\bar{x})|d\bar{x}$, while the other half is $(\delta/I)\int_{0.5}^{1}|j(\bar{x})|d\bar{x}$. By taking a linear approximation, we can further express the two integrals, given that $j(\bar{x})$ is negative
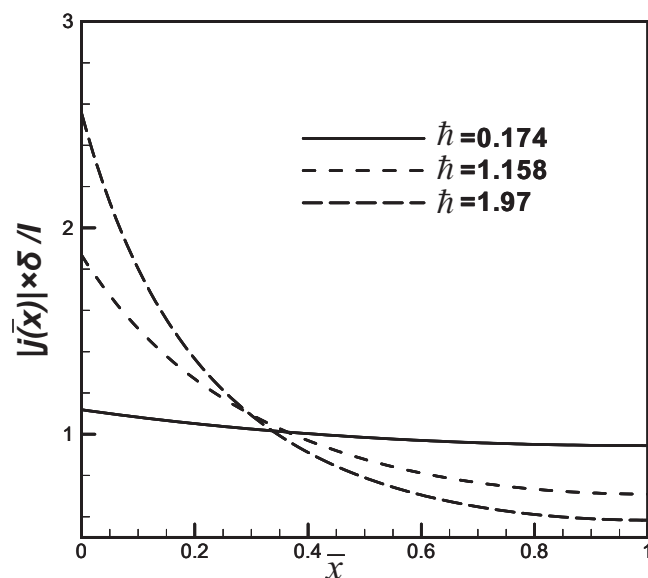

Figure 7. Spatial variation of the reaction current densities at different $\hbar$ values.

Conclusions

This paper investigated the transport and electrochemical phenomena within the cathode electrode of PEFCs. Theoretical analysis indicated that the spatial variations of temperature, oxygen concentration, water content, and ionic conductivity across the electrode are small and negligible. A 1D model of the electrochemical kinetics in the cathode was further developed and theoretical solutions of the electrolyte phase potential and local transfer current density were obtained explicitly. It is found that the distributions of local electrolyte phase potential and reaction rate relates to a lumped parameter $\Delta U^{j\delta}$. This lumped parameter combines the impacts of a number of parameters, including composite properties, electrode structure, and electrode thickness, which are of importance practical for electrode fabrication and optimization. In addition, a variable $\hbar$ was defined to characterize the reaction rate spatial variation across the cathode and found as a linear function of another lumped factor ΔU, which combines the effects of overall electrode ionic resistance R_δ and average current density I. The factor $\hbar$ can be used to probe the degree of spatial variation of electrode local reaction rates and catalyst utilization, as well as a criterion to assess the validity of assuming a uniform reaction across the electrode that is frequently adopted in electrode analyses. In addition, the obtained exact solutions can be

applied to develop efficient multidimensional models of electrodes, as distributions of the key quantities in the thickness dimension can be explicitly expressed.

List of Symbols

a	effective catalyst area per unit volume, m^2/m^3	
a_o	catalyst surface area per unit volume, m^2/m^3	
C	molar concentration of species k, mol/m^3	
D	species diffusivity, m^2/s	
F	Faraday's constant, 96,487 C/equiv	
$\hbar$	nonuniformity	
I	current density, A/cm^2	
i	superficial current density, A/cm^2	
j	transfer current density, A/cm^3	
k	thermal conductivity, W/m K	
M	molecular weight, kg/mol; molecular diffusion	
P	pressure, Pa	
R	ohmic resistance, $m\Omega$ cm^2	
R_g	universal gas constant, 8.134 J/mol K	
T	temperature, K	
U_o	equilibrium potential, V	

Greek

α	transfer coefficient; net water flux per proton flux	
ρ	density, kg/m^3	
ν	kinetic viscosity, m^2/s	
Φ	phase potential, V	
σ	conductivity, S/m; surface tension, N/m	
θ_c	contact angle, °	
λ	membrane water content	
ε	porosity	
η	surface overpotential, V	
τ	tortuosity	
δ	thickness, m	

Superscripts and Subscripts

c	cathode; capillary
d	diffusion
eff	effective value
g	gas phase
m	membrane phase
o	reference value
ref	reference value
s	solid
sat	saturate value

References

1. T. E. Springer, T. A. Zawodzinski, and S. Gottesfeld, *J. Electrochem. Soc.*, **138**, 2334 (1991).
2. T. E. Springer, M. S. Wilson, and S. Gottesfeld, *J. Electrochem. Soc.*, **140**, 3513 (1993).
3. C. Boyer, S. Gamburzev, O. Velev, S. Srinivasan, and A. J. Appleby, *Electrochim. Acta*, **43**, 3703 (1998).
4. G. C. Li and P. G. Pickup, *J. Electrochem. Soc.*, **150**, C745 (2003).
5. K. C. Neyerlin, W. Gu, J. Jorne, A. Clarke, Jr., and H. A. Gasteiger, *J. Electrochem. Soc.*, **154**, B279 (2007).
6. C. C. Boyer, R. G. Anthony, and A. J. Appleby, *J. Appl. Electrochem.*, **30**, 777 (2000).
7. V. Gurau, F. Barbir, and H. Liu, *J. Electrochem. Soc.*, **147**, 2468 (2000).
8. Y. Wang and C. Y. Wang, *J. Electrochem. Soc.*, **152**, 445 (2005).
9. A. Rowe and X. Li, *J. Power Sources*, **102**, 82 (2001).
10. H. Ju, H. Meng, and C. Y. Wang, *Int. J. Heat Mass Transfer*, **48**, 1303 (2005).
11. S. Mazumder and J. V. Cole, *J. Electrochem. Soc.*, **150**, 1510 (2003).
12. U. Pasaogullari and C. Y. Wang, *Electrochim. Acta*, **49**, 4359 (2004).
13. H. Meng, *J. Power Sources*, **162**, 426 (2006).
14. G. Lin and T. Van Nguyen, *J. Electrochem. Soc.*, **153**, A372 (2006).
15. Y. Wang and C. Y. Wang, *J. Electrochem. Soc.*, **153**, A1193 (2006).
16. Y. Wang and C. Y. Wang, *Electrochim. Acta*, **50**, 1307 (2005).
17. M. Eikerling, *J. Electrochem. Soc.*, **153**, E58 (2006).
18. Y. Wang and C. Y. Wang, *Electrochim. Acta*, **51**, 3924 (2006).
19. Q. P. Wang, M. Eikerling, D. T. Song, and Z. S. Liu, *J. Electrochem. Soc.*, **154**, 95 (2007).
20. P. K. Das, X. Li, and Z. S. Liu, *J. Electroanal. Chem.*, **604**, 72 (2007).
21. A. Z. Weber and J. Newman, *J. Electrochem. Soc.*, **154**, B405 (2007).
22. G. Wang, P. P. Mukherjee, and C. Y. Wang, *Electrochim. Acta*, **52**, 6367 (2007).
23. Y. Wang, *J. Electrochem. Soc.*, **154**, B1041 (2007).
24. A. Parthasarathy, S. Srinivasan, and A. J. Appleby, *J. Electrochem. Soc.*, **139**, 2530 (1992).
25. S. Motupally, A. J. Becker, and J. W. Weidner, *J. Electrochem. Soc.*, **147**, 3171 (2000).
26. T. Berning and N. Djilali, *J. Electrochem. Soc.*, **150**, A1589 (2003).